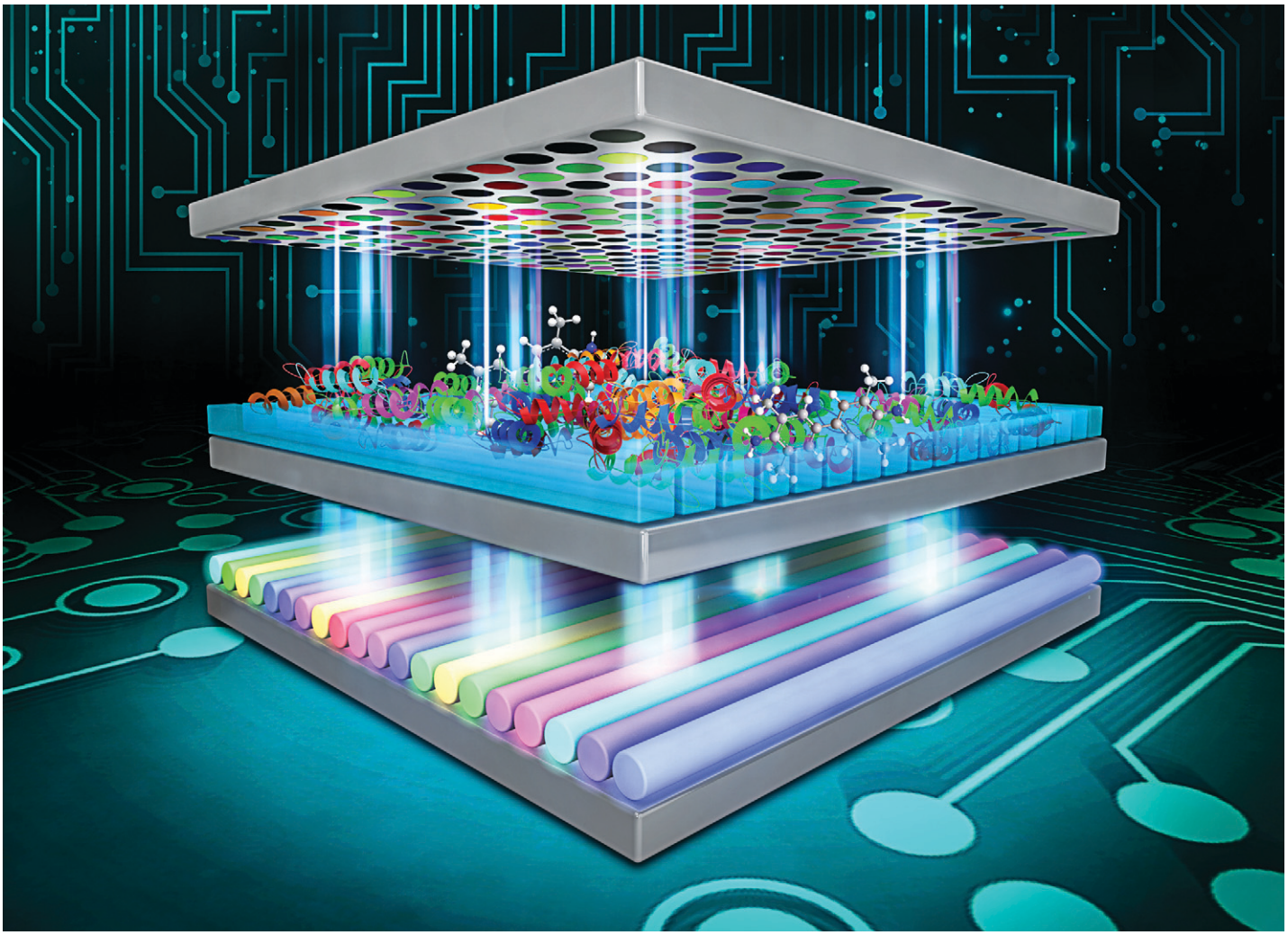

Featuring work from Professor Yuan Gong and Professor Yun-Jiang Rao, University of Electronic Science and Technology of China (UESTC), China.

Distributed fibre optofluidic laser for chip-scale arrayed biochemical sensing

The concept of a distributed fibre optofluidic laser was proposed and demonstrated in a chip-scale arrayed sensor. The concentration of the enzyme HRP was detected by arrayed colorimetric detection and parallel imaging. This work paves the way towards optofluidic laser-based high-throughput biochemical sensing.

As featured in:

See Yuan Gong, Gang-Ding Peng, Yun-Jiang Rao *et al.*, *Lab Chip*, 2018, **18**, 2741.

ROYAL SOCIETY OF CHEMISTRY

rsc.li/loc

Registered charity number: 207890

Lab on a Chip

PAPER

View Article Online
View Journal | View Issue

Cite this: *Lab Chip*, 2018, **18**, 2741

Distributed fibre optofluidic laser for chip-scale arrayed biochemical sensing†

Chaoyang Gong,[a] Yuan Gong, *[a] Xuhao Zhao,[a] Yanhua Luo,[b] Qiushu Chen,[c] Xiaotian Tan, [c] Yu Wu,[a] Xudong Fan, [c] Gang-Ding Peng*[b] and Yun-Jiang Rao*[a]

Received 22nd June 2018,
Accepted 3rd August 2018

DOI: 10.1039/c8lc00638e

rsc.li/loc

Optofluidic lasers (OFLs) are an emerging technological platform for biochemical sensing, and their good performance especially high sensitivity has been demonstrated. However, high-throughput detection with an OFL remains a major challenge due to the lack of reproducible optical microcavities. Here, we introduce the concept of a distributed fibre optofluidic laser (DFOFL) and demonstrate its potential for high-throughput sensing applications. Due to the precise fibre geometry control *via* fibre drawing, a series of identical optical microcavities uniformly distributed along a hollow optical fibre (HOF) can be achieved to obtain a one-dimensional (1D) DFOFL. An enzymatic reaction catalysed by horseradish peroxidase (HRP) can be monitored over time, and the HRP concentration is detected by DFOFL-based arrayed colorimetric detection. Experimentally, five-channel detection in parallel with imaging has been demonstrated. Theoretically, spatial multiplexing of hundreds of channels is achievable with DFOFL-based detection. The DFOFL wavelength is tuned over hundreds of nanometers by optimizing the dye concentration or reconfiguring the liquid gain materials. Extending this concept to a two-dimensional (2D) chip through wavelength multiplexing can further enhance its multi-functionality, including multi-sample detection and spectral analysis. This work opens the door to high-throughput biochemical sensing.

Introduction

Optofluidics, which integrates photonics and microfluidics, has attracted much attention for miniature lab-on-a-chip or micro-total-analysis-system applications.[1–6] An optofluidic laser (OFL)[7] is a valuable tool for cell tagging[8,9] or biosensing[10,11] and can be used as an on-chip laser source.[12] To date, various optical feedback mechanisms for OFLs have been explored, including whispering-gallery mode (WGM) microcavities based on capillaries,[13] microbeads,[14] on-chip or in-fiber ring resonators,[15,16] microbottles,[17,18] microdroplets,[19] Fabry–Pérot (FP) resonators[11,20,21] and random scattering.[22,23] For biochemical detection, OFL sensors with ultrahigh sensitivity have been reported.[7,10,11,20] However, high-throughput biochemical sensing based on OFLs remains a major challenge.

High-throughput sensing is critical for biological diagnostics,[24–26] DNA sequencing[27,28] and drug screening.[29,30] Efforts to develop an OFL array have paved the way towards high-throughput capabilities. On-chip microresonators were employed for arrayed OFLs since they can be mass-produced in parallel with a high Q factor and compactness.[31–33] Microresonators were also employed through reflective microwells in an FP cavity to achieve an OFL array.[34,35] These arrayed microresonators hold the non-uniform geometry from batch to batch that leads to the fluctuations in optical properties and hinders the potential of OFLs for high-throughput sensing applications.[36]

In this paper, we report a distributed fibre optofluidic laser (DFOFL) with uniform lateral emission based on a hollow core optical fibre (HOF). The DFOFL is utilized as a light source for chip-scale multi-channel biochemical sensing. The superiority of the proposed optofluidic laser is three-fold. First, the uniformly distributed spatial distribution of the DFOFL enables on-chip arrayed detection *via* various microfluidic channels. The cylindrical structure of the HOF supports a continuous series of WGM microcavities distributed along the fibre axis. Due to precise control of the fibre geometry during the drawing process, these microcavities have identical diameters and surface roughness values, leading to a uniform laser-emission distribution. Second, utilizing the reconfigurability of a liquid, the DFOFL wavelength can be

[a] *Key Laboratory of Optical Fiber Sensing and Communications (Ministry of Education of China), University of Electronic Science and Technology of China, No. 2006, Xiyuan Ave., Chengdu, 611731 China. E-mail: ygong@uestc.edu.cn, yjrao@uestc.edu.cn*

[b] *School of Electrical Engineering and Telecommunications, University of New South Wales, Sydney, NSW 2052, Australia. E-mail: g.peng@unsw.edu.au*

[c] *Department of Biomedical Engineering, University of Michigan, 1101 Beal Ave., Ann Arbor, MI 48109, USA*

† Electronic supplementary information (ESI) available. See DOI: 10.1039/c8lc00638e

tuned over hundreds of nanometers to optimize the sensing performance, making the DFOFL more compact and flexible than conventional light sources. Third, because of the narrow emission band of the DFOFL, wavelength multiplexing of the DFOFL can also be implemented, which may give rise to a multifunctional 2D chip. After spectrally and spatially characterizing the DFOFL, chip-scale arrayed sensing of the horseradish peroxidase (HRP) enzyme is experimentally demonstrated. The 2D array of sensors with multiple functionalities is also investigated. The proposed DFOFLs and arrayed sensors are easy to use and fabricate and are promising for high-throughput biochemical sensing.

Experimental

Fabrication of the HOF

Hollow fibre drawing was performed on a fibre drawing apparatus (Controls Interface) in the University of New South Wales (UNSW). The hollow fibre was drawn from a quartz tube (Heraeus F300, thickness of 1.5 mm, O.D. = 25 mm) mounted on the feeder of the draw tower. Then, the tube was slowly fed into a graphite furnace heated and melted into the fibre with capstan drawing. The hollow fibre dimensions were controlled by the drawing temperature, T, tube feeding rate, V_f, fibre drawing rate, V_d, and internal pressure, P, which was applied by the flow rate of high-purity nitrogen purged into the tube. Typical fabrication conditions are T = 1900 °C, V_f = 0.5 mm min^{-1}, V_d = 5 m min^{-1} and P = 1.3 mbar. The inner and outer diameters of the resulting HOF were 32 μm and 99 μm, respectively (Fig. 1a). In addition, the bare hollow fiber was protected by a UV-curable coating (DeSolite 3471-3-14). The fiber geometry can be well controlled by the fiber draw tower. The HOF with a large diameter may withdraw too much bulk gain solution and will result in a strong fluorescence background. In this work, because of the high refractive index of quinoline (n = 1.63) filled in the HOF, optical feedback was provided by the whispering gallery mode (WGM) on the silica–liquid interface. In principle, there is no requirement for the fiber thickness. Considering the frangibility of the thin wall optical fiber, the HOF with a thickness of over 20 μm is robust for handling.

Reagents

A chromogenic reaction was used as a model to demonstrate the sensing capability of the device. A transparent substrate, 3,3′,5,5′-tetramethylbenzidine (TMB), was catalysed by the HRP enzyme to produce colour changes in bulk solution. In immunodiagnostics, such as enzyme-linked immunosorbent assay (ELISA), TMB has been widely used as a colour-changing label for biomarker detection.[37–39] The reaction product has strong absorption between 600 nm and 700 nm.[40] The salt-free lyophilized HRP powder (No. 31490) was purchased from ThermoFisher. The stabilized hydrogen peroxide (colour reagent A, No. 895000) and stabilized TMB (colour reagent B, No. 895001) were purchased from R&D System. Laser dyes, including Rhodamine 6G (R6G, No. 05901), Rhodamine 640 (Rh640, No. 06400), and HITC (No. 08421), were purchased from Exciton.

1D-DFOFL

A 1D-DFOFL was fabricated based on the HOF. The HOF (length, 25 mm) was sonicated in acetone for 5 min to remove the polymer coating. The bare HOF was sequentially washed with acetone and ethanol for 5 min, followed by deionized water three times. Rhodamine 6G (R6G) in quinoline

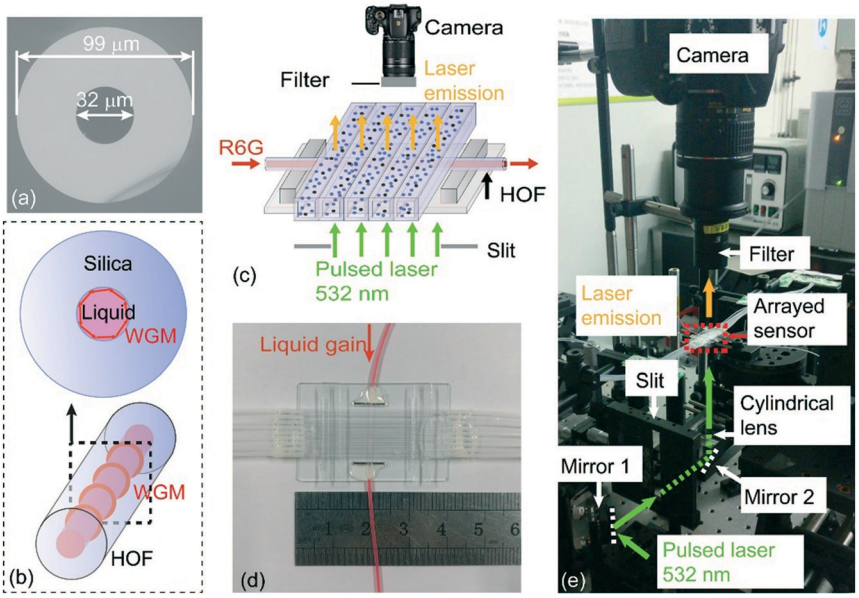

Fig. 1 (a) SEM image of the HOF cross-section. (b) Illustration of the optical microcavities in the cross-section (top) and continuously distributed along the fibre (bottom). (c) Schematic diagram and (d) photo of the chip-scale arrayed sensor. (e) Photo of the experimental setup for the distributed fibre optofluidic laser.

(n = 1.63), as the gain medium, was drawn into the HOF using a syringe pump. Due to the large refractive index difference between quinoline and silica, total internal reflection occurs at the HOF–liquid interface, creating an in-fibre microresonator for lasing (top, Fig. 1b). The HOF's cylindrical structure allows an array of microcavities to be continuously distributed in the longitudinal direction (bottom, Fig. 1b). Because the fibre draw tower can precisely control the fibre geometry, these distributed microcavities were uniform. When these dye-filled microcavities were simultaneously excited using a pump strip, a 1D distributed lateral laser emission along the fibre can be obtained. The light beam from a 532 nm pulsed laser (Continuum, 5 ns pulse width, 20 Hz repetition rate) was expanded and then focused by a cylindrical lens to form a strip to pump the DFOFL (Fig. 1e). The output of the pump laser is a top-hat beam as a variable reflective mirror with a Gaussian reflection distribution was used in the laser. Further, the pump laser beam was expanded and spatially filtered using a tunable slit (7 mm) to select the central uniform region. The 1D-DFOFL spectra were measured using a spectrometer (Andor, SR500IA). The laser wavelength can be adjusted by reconfiguring the microfluidic dye.

Chip-scale DFOFL sensor

Silica capillaries (inner square cross-section: 1 mm × 1 mm, thickness: 176 μm) were used as microfluidic channels for sensing. Five capillaries were integrated perpendicular to the 1D distributed optofluidic laser to form a chip-scale sensing array (Fig. 1c and d). The DFOFL laser emission was absorbed by the reagent in the capillaries. A commercial camera (Nikon, D3400, Fig. 1e) was used to collect the transmitted laser emission. Due to the lateral laser emission, the camera was placed perpendicularly to the fiber axis. By tuning the collection lens, the FOFL was clearly imaged on the camera and thus the intensity distribution on the FOFL was recorded precisely. By monitoring the DFOFL transmission, the catalytic reaction in each channel can be simultaneously monitored.

Results and discussion

Numerical simulations

The optical resonance in the WGM microcavity was numerically simulated by the finite element method (FEM). Fig. 2a shows the intensity distribution in the HOF cross-section. A bright circle of intensity resonance is obtained on the HOF–liquid interface. The enlargement presented in Fig. 2b shows that the optical resonance is almost completely confined in the liquid due to its refractive index being higher than that of silica, which enables strong light–matter interaction and results in a low lasing threshold. The light intensity at the outer surface of the HOF is almost zero, indicating that no optical resonance occurs in the micro-ring at the HOF–air interface.

In the chip-scale OFL sensor, the concentration of the product from the catalytic reaction and the corresponding absorption increase as the reaction occurs. The OFL transmission through the capillaries decreases according to the Beer–Lambert law,[41]

$$T = 10^{-\alpha LC}, \quad (1)$$

where α is the molar attenuation coefficient of the product, L is the thickness of the solution through which the light

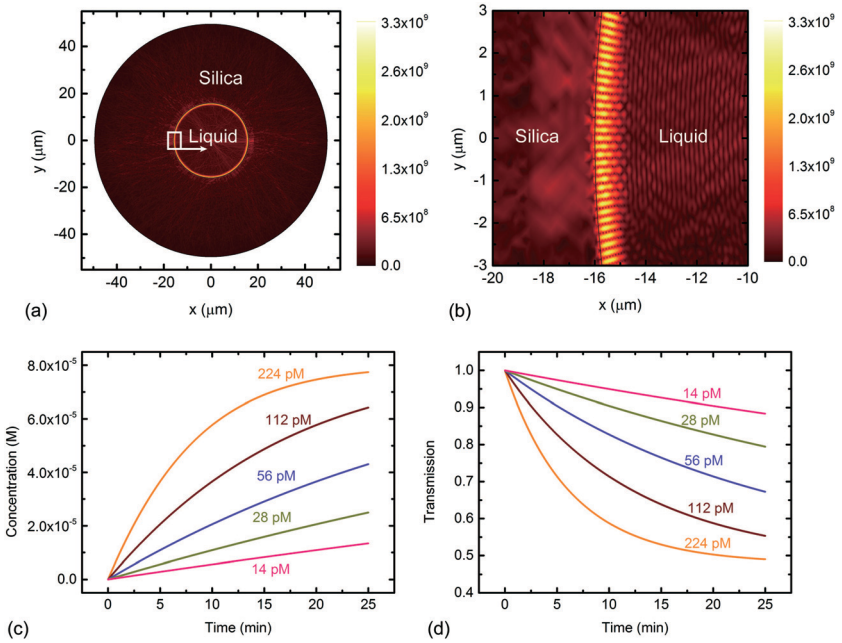

Fig. 2 (a) Numerical simulation of the intensity distribution in the HOF cross-section and (b) its enlargement. (c) Simulated product concentrations and (d) OFL transmission *versus* reaction time.

passes, and C is the concentration of the product, which can be calculated using the Michaelis–Menten equation (see the ESI† for details). Fig. 2c shows that the product concentration increases with time, t, and the reaction rate speeds up with increasing HRP concentration. The C–t curve deviates from a linear trend at higher HRP concentrations due to consumption of the substrate. The corresponding OFL transmission as a function of the reaction time is plotted in Fig. 2d, and these predictions are consistent with the experimental results.

DFOFL performance

Spectra and threshold. The threshold of the 1D optofluidic laser was characterized by recording the laser spectra at various pump energy densities (Fig. 3a). Due to the strong light–liquid interaction and high Q factor of the WGM microcavity, a low threshold of 0.5 μJ mm^{-2} was achieved (Fig. 3b). Note that the threshold was measured for the whole 1D optofluidic laser that was continuously distributed over 7 mm, and thus, the threshold was an average value. The free spectral range (FSR) of the laser emission was approximately 2.25 nm. This result is in good agreement with the theoretical prediction, 2.28 nm, which was calculated by FSR = $\lambda^2/(n\pi d)$ where λ = 620 nm is the lasing wavelength, n = 1.63 is the refractive index of the liquid gain material, and d = 32.9 μm is the HOF inner diameter measured from the SEM image. The excellent consistency of the experimental and theoretical FSR values confirmed that the optical feedback was provided by the resonance of the WGM microcavity at the HOF–liquid interface. The residual difference in the FSR may be a result of the slightly lower effective index of the WGM than the index of quinoline. With a pump density below the threshold, weak, broad fluorescence peaks were observed (grey curve, inset of Fig. 3b, P = 0.4 μJ mm^{-2}). With increasing pump density, laser peaks emerged with intensities two orders of magnitude higher than that of the fluorescence peak (orange curve, inset of Fig. 3b, P = 2.4 μJ mm^{-2}). The full width at half maximum (FWHM) of the laser emission was about 4.7 nm, which is much narrower than those of traditional halogen tungsten lamps and LEDs.

Spatial distribution. The DFOFL spatial distribution, especially the longitudinal distribution uniformity, determines its arrayed sensing performance. When 10 mM R6G in quinoline was used, a central laser wavelength of 620 nm was obtained. A long pass filter with a cutting wavelength of 610 nm and a neutral density filter (OD = 2) were utilized to filter the fluorescence. The 3D distribution of the laser intensity (Fig. 3c), which was recovered from the corresponding photograph (inset, Fig. 3d), was recorded from a single pulse. A Gaussian transverse distribution was obtained (top, Fig. 3d). The longitudinal distribution of the laser emission was uniform (bottom, Fig. 3d) with a transverse position at x = 22.5 μm, which originated from the same inner diameter along the HOF and consistently distributed WGM microcavities. The standard deviation of the intensity, σ = 6.6%, resulted from the inhomogeneity of the pump laser intensity distribution.

DFOFL-based sensing array

Colorimetric detection of HRP. Chip-scale sensing of the HRP enzyme was performed by colorimetric detection using the DFOFL as the light source. For a better sensing

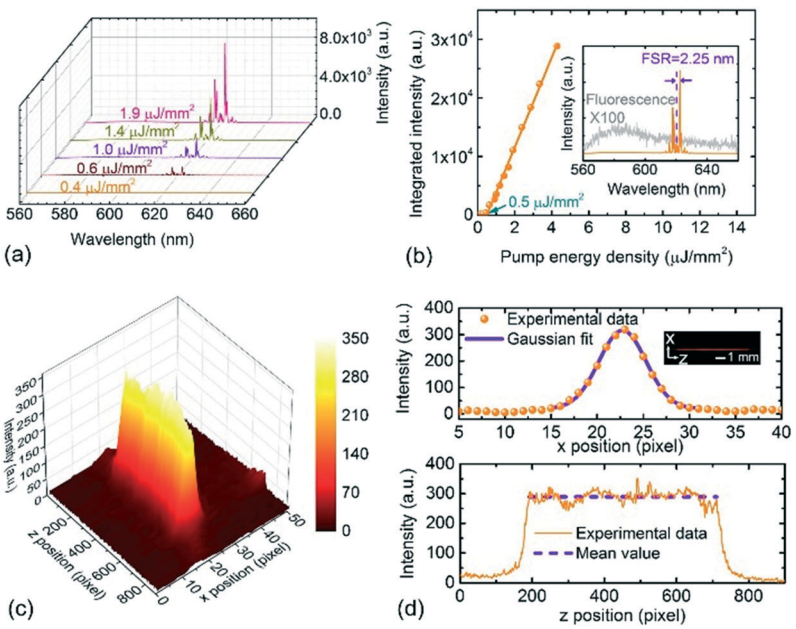

Fig. 3 (a) The emission spectra of the DFOFL with various pump densities. (b) The integrated intensity as a function of the pump energy density, showing a low threshold of 0.5 μJ mm^{-2}. The spectra are integrated from 610 nm to 630 nm. Inset: Laser spectra at 2.4 μJ mm^{-2} and the fluorescence (×100 for clearance) at 0.4 μJ mm^{-2}. (c) 3D plot of the DFOFL intensity distribution with the corresponding transverse (top) and longitudinal (bottom) distributions in (d). Inset of (d), photograph of the DFOFL.

performance, the DFOFL wavelength was tuned to 620 nm by optimizing the gain material concentration (described in the next section) to match the catalytic product absorbance. Images of the DFOFL were recorded *versus* time after drawing the working substrate and HRP mixture into the microfluidic channel. The protocol for preparing the reagents is given in the ESI.† The substrate becomes blue after mixing with HRP, and its absorption increases; thus, the transmission decreases according to the Beer–Lambert law. Fig. 4a shows the DFOFL transmission intensity distribution at t = 0 min and t = 10 min (photograph in the inset). Two stable side peaks can clearly be used to identify the inner surfaces of the square capillary.

The transmission was calculated as the integral of the intensity between the two side peaks and is shown as a function of the reaction time (Fig. 4b). The substrate concentration was initially sufficient, and the transmission linearly decreased over time. As the reaction continued, the decrease in the transmission slowed down and finally terminated at a higher enzyme concentration because the substrate was completely catalysed. The slope in Fig. 4b increases with increasing HRP concentration. We utilized the specific reaction time as the sensing signal, defined as the time when the transmission decreases to 90% of the original intensity. Fig. 4c shows the specific reaction time as a function of the enzyme concentration, and this plot can be used as the HRP calibration curve. HRP was prepared at concentrations between 14 pM and 224 pM by 2-fold serial dilution. The lower limit of detection (LOD) was 14 pM. HRP concentrations in this range are frequently utilized in bioassays.[42,43]

Uniform chip-scale sensing array. Another advancement in this work was the development of arrayed enzyme sensors based on the 1D-DFOFL that can detect samples in parallel. A chip-scale sensing array was fabricated (Fig. 1e). The photograph (inset of Fig. 4d) shows in parallel the DFOFL transmission through five microfluidic channels at reaction times 0 and 10 min with the corresponding extracted intensity distribution of each channel (Fig. 4e). In this experiment, each channel was filled with the same substrate and HRP mixture (224 pM) to demonstrate the reproducibility of the different channels as consistent elements for arrayed sensors. The photo clearly shows five regions, which are periodically bright and dark. The uniform output from the five channels was confirmed by calculating the transmission of each channel (Fig. 4d) with a standard deviation of approximately 7%, which mainly originated from the inhomogeneity of the pump beam and capillary width.

Evaluation of maximum arrayed channels. Similar to distributed fibre-optic sensors based on optical time-domain reflectometry (OTDR),[44] the maximum arrayed channels in a chip can be estimated by the length of the DFOFL as well as the spatial resolution. For chip-scale applications, a DFOFL with a length of 20 mm can be easily achieved by expanding a flat-top pump strip. To further extend the DFOFL length, we propose a bi-directional pumping method through both fibre ends of a microstructured optical fibre, which can support pump beam transmission in the core and allow the pump to interact with the liquid gain material in the cladding holes (Fig. S1, ESI†).

The spatial resolution is mainly determined by the width of the capillaries or microfluidic channels, as well as the pixels of the camera. Considering the current fabrication facilities, the width of each channel can be easily reduced to 50 μm with glass capillaries or a microfluidic chip, allowing up to 400 sensing channels to be integrated into a chip with a length of 2 cm. On the other hand, commercial cameras

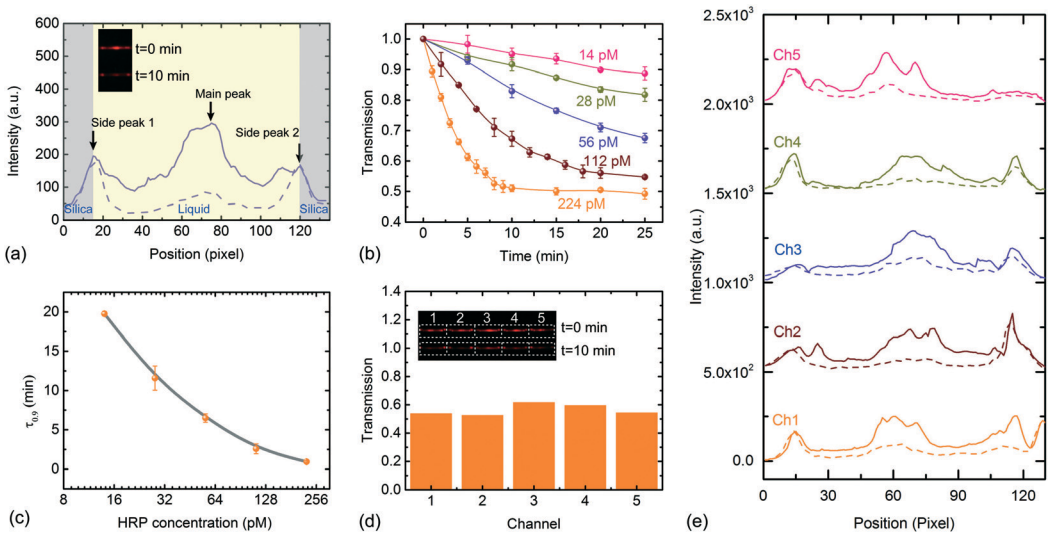

Fig. 4 (a) DFOFL transmission intensity distribution at reaction time 0 (solid) and 10 min (dotted). (b) Transmission as a function of the reaction time for different HRP concentrations. (c) Specific reaction time *versus* HRP concentration. Data were derived from (b). (d) The DFOFL uniform transmission through five channels with the same catalytic reaction time of 10 min and (e) the corresponding intensity distribution. The HRP concentration was 224 pM in (a), (d) and (e). The intensity curves are vertically offset for clarity. Insets: Photographs of DFOFL transmission through the microfluidic channels.

with 16 megapixels commonly have 4000 pixels in 1D, enabling at least 100 detection channels with 40 pixels each. Further extension of channels may be achieved by an image splicing method.

Extension to 2D by wavelength multiplexing

Wavelength tunability over 250 nm. After estimating the spatial multiplexing of ~100 channels with one DFOFL, we attempted to further extend the DFOFL multi-functionality *via* the concept of wavelength-division multiplexing (WDM). The idea of WDM has been widely utilized in optical fibre communications, fibre Bragg grating sensor networking and fluorescent label bioimaging with different colours.[45–47] Here, we use the reconfigurability of microfluidics to develop DFOFLs with multiple wavelengths and propose a design to construct a 2D microfluidic chip.

Optofluidic lasers can be tunable over a wide range by either adjusting the concentration or using different liquid gain materials. As shown in Fig. 5a, the lasing peaks shift to longer wavelengths, *i.e.*, from 580 nm to 620 nm, with increasing R6G concentration due to fluorescence reabsorption,[48] which increases micro-ring resonator losses in the shorter wavelength range. The wavelength tunability with a certain gain material is limited by the lowest concentration that enables lasing as well as the saturated concentration.

The lasing wavelength can be extended to the near infrared (NIR) region based on the Förster resonance energy transfer (FRET) method. The donor Rh640 and acceptor HITC were dissolved in quinoline at concentrations of 8 mM and 2.5 mM, respectively. The mixture was drawn into the HOF as the gain medium. In the absence of HITC, lasing was observed at approximately 640 nm using Rh640 as the gain material. Upon mixing the donor and acceptor, the excited Rh640 molecule emits a virtual photon that is instantly absorbed by the HITC molecule. The FRET optofluidic laser began to lase at a threshold of 1.9 μJ mm^{-2}. The laser wavelength was extended to 825 nm (Fig. 5a), and a wavelength tunability range of over 250 nm was demonstrated. Even a wider tuning range can be obtained by exploring other types of dyes or photoluminescent nanomaterials.[49]

2D microfluidic chip with multiple functionalities. The concept of the 1D-DFOFL can be extended to a 2D microfluidic chip by multiplexing multiple 1D-DFOFLs with various wavelengths (λ_1–λ_n), and for each wavelength, spatial multiplexing (Ch. 1–Ch. *n*) can be simultaneously implemented by vertical integration (inset of Fig. 5a). In order to avoid spectral overlap, the spectral resolution is estimated to be about 10 nm (Fig. 5a). Considering the spectral coverage of 250 nm demonstrated here, 25 DFOFLs can be multiplexed. The 2D chip pattern recorded by the camera forms a "dot array" (Fig. 5b), consisting of up to 2500 sensing elements (with 100 detection channels estimated for each wavelength).

The proposed optofluidic chip has several advantages compared with the existing arrayed biochemical sensors including those based on fluorescence imaging and arrayed ELISA. Firstly, thanks to the narrow linewidth and uniform spatial distribution of the 1D-FOFLs, spatial and spectral multiplexing of more than a thousand sensing elements on a 2D chip are available. Comparatively, fluorescence often has a wide emission bandwidth, which limits the spectral multiplexing capability. Secondly, compared with 96-well plate based assays such as ELISA, the microfluidic channels are small in size and have at least 10 times lower volume sample consumption. Thirdly, its multi-functionality enables

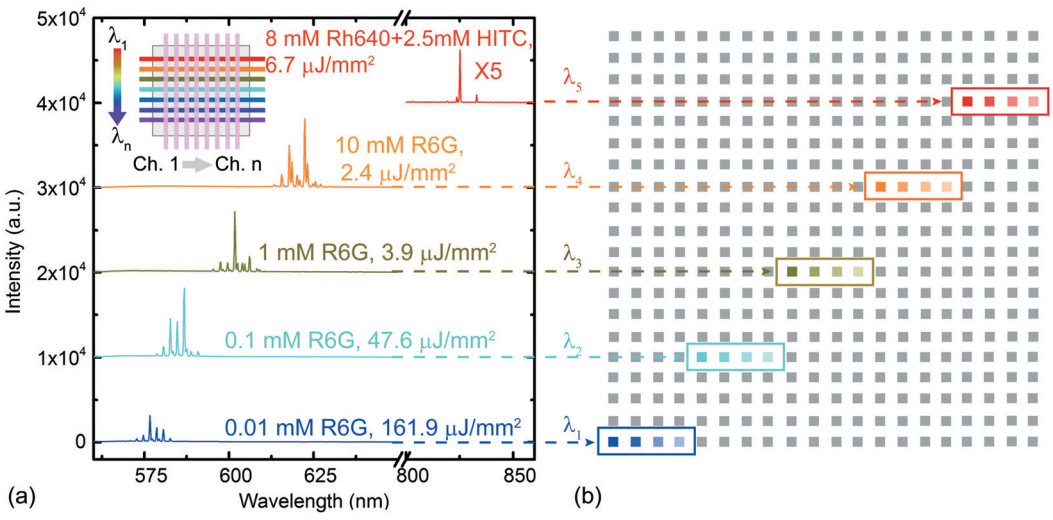

Fig. 5 (a) Laser spectra of DFOFLs. Lasing between 580 nm to 620 nm was achieved at various R6G concentrations. The energy density for pumping R6G was roughly adjusted to obtain a similar laser intensity. Lasing at approximately 820 nm can be achieved based on the FRET effect between Rh640 and HITC. Inset: Illustration of the 2D microfluidic chip concept based on DFOFLs with different wavelengths and spatial multiplexing. The spectral curves are vertically offset for clarity. (b) Schematic diagram of colorimetric detection of different samples based on 2D-DFOFL chips. Each colour indicates one type of sample, and the brightness varies with the concentration.

the optofluidic chip to be a useful platform. Arrayed concentration detection is demonstrated in Fig. 4. Monitoring of bio/chemical reactions in real time can also be performed by recording the temporal changes of laser intensity (Fig. 4b). Further, various analytes can be detected simultaneously by wavelength multiplexing, illustrated by different coloured boxes in Fig. 5b. The transmission of different FOFLs through the same channel could give absorption spectral information for certain analytes (Fig. S2, ESI†).

Conclusions

The concept of distributed fibre optofluidic lasers has been introduced and implemented utilizing HOFs. The HOF offers continuously distributed, identical WGM microcavities along the fibre, resulting in a uniformly distributed lateral laser emission. The 1D-DFOFL was integrated with microfluidic channels for chip-scale arrayed sensing of the HRP enzyme by imaging. The wavelength tunability over hundreds of nanometers was explored for future high-throughput and multifunctional biochemical sensing applications that utilize both wavelength and spatial multiplexing in a 2D microfluidic chip.

Conflicts of interest

There are no conflicts of interest to declare.

Acknowledgements

We acknowledge financial support from the National Natural Science Foundation of China (61575039), the 111 Project (B14039), and the National Science Foundation (DBI-1451127).

References

1 D. Psaltis, S. R. Quake and C. Yang, *Nature*, 2006, **442**, 381–386.
2 H. Schmidt and A. R. Hawkins, *Nat. Photonics*, 2011, **5**, 598–604.
3 U. Hassan, T. Ghonge, B. Reddy, Jr, M. Patel, M. Rappleye, I. Taneja, A. Tanna, R. Healey, N. Manusry, Z. Price, T. Jensen, J. Berger, A. Hasnain, E. Flaugher, S. Liu, B. Davis, J. Kumar, K. White and R. Bashir, *Nat. Commun.*, 2017, **8**, 15949.
4 H. Craighead, *Nature*, 2006, **442**, 387–393.
5 B. H. Wunsch, J. T. Smith, S. M. Gifford, C. Wang, M. Brink, R. L. Bruce, R. H. Austin, G. Stolovitzky and Y. Astier, *Nat. Nanotechnol.*, 2016, **11**, 936–940.
6 C. Lin, C. Liao, Y. Zhang, L. Xu, Y. Wang, C. Fu, K. Yang, J. Wang, J. He and Y. Wang, *Lab Chip*, 2018, **18**, 595–600.
7 X. Fan and S. H. Yun, *Nat. Methods*, 2014, **11**, 141–147.
8 M. C. Gather and S. H. Yun, *Nat. Photonics*, 2011, **5**, 406–410.
9 M. Humar and S. H. Yun, *Nat. Photonics*, 2015, **9**, 572–576.
10 Y. C. Chen, X. Tan, Q. Sun, Q. Chen, W. Wang and X. Fan, *Nat. Biomed. Eng.*, 2017, **1**, 724–735.
11 X. Wu, M. K. K. Oo, K. Reddy, Q. Chen, Y. Sun and X. Fan, *Nat. Commun.*, 2014, **5**, 3779.
12 A. J. C. Kuehne, M. C. Gather, I. A. Eydelnant, S. H. Yun, D. A. Weitz and A. R. Wheeler, *Lab Chip*, 2011, **11**, 3716–3919.
13 Q. Chen, A. Kiraz and X. Fan, *Lab Chip*, 2016, **16**, 353–359.
14 M. Humar, A. Dobravec, X. Zhao and S. H. Yun, *Optica*, 2017, **4**, 1080–1085.
15 M. Ren, H. Cai, L. K. Chin, K. Radhakrishnan, Y. Gu, G. Q. Lo, D. L. Kwong and A. Q. Liu, *Optica*, 2015, **2**, 940–943.
16 L. Shi, T. Zhu, D. Huang, M. Liu, M. Deng and W. Huang, *Opt. Lett.*, 2015, **40**, 3770–3773.
17 F. Gu, F. Xie, X. Lin, S. Linghu, W. Fang, H. Zeng, L. Tong and S. Zhuang, *Light: Sci. Appl.*, 2017, **6**, e17061.
18 M. Sumetsky, *Light: Sci. Appl.*, 2017, **6**, e17102.
19 D. McGloin, *Rep. Prog. Phys.*, 2017, **80**, 054402.
20 C. Gong, Y. Gong, M. K. K. Oo, Y. Wu, Y. Rao, X. Tan and X. Fan, *Biosens. Bioelectron.*, 2017, **96**, 351–357.
21 C. Y. Gong, Y. Gong, W. L. Zhang, Y. Wu, Y. J. Rao, G. D. Peng and X. Fan, *IEEE J. Sel. Top. Quantum Electron.*, 2018, **24**, 0900206.
22 N. Bachelard, S. Gigan, X. Noblin and P. Sebbah, *Nat. Phys.*, 2014, **10**, 426–431.
23 J. Liu, P. D. Garcia, S. Ek, N. Gregersen, T. Suhr, M. Schubert, J. Mørk, S. Stobbe and P. Lodahl, *Nat. Nanotechnol.*, 2014, **9**, 285–289.
24 L. J. Wang, Y. C. Chang, R. Sun and L. Li, *Biosens. Bioelectron.*, 2017, **87**, 686–692.
25 X. P. He, X. L. Hu, T. D. James, J. Yoon and H. Tian, *Chem. Soc. Rev.*, 2017, **46**, 6687–6696.
26 A. E. Cetin, A. F. Coskun, B. C. Galarreta, M. Huang, D. Herman, A. Ozcan and H. Altug, *Light: Sci. Appl.*, 2014, **3**, e122.
27 J. A. Reuter, D. V. Spacek and M. P. Snyder, *Mol. Cell*, 2015, **58**, 586–597.
28 V. S. Chambers, G. Marsico, J. M. Boutell, M. D. Antonio, G. P. Smith and S. Balasubramanian, *Nat. Biotechnol.*, 2015, **33**, 877–881.
29 X. Li, X. Zhang, S. Zhao, J. Wang, G. Liu and Y. Du, *Lab Chip*, 2014, **14**, 471–481.
30 H. A. Kenny, M. Lal-Nag, E. A. White, M. Shen, C. Y. Chiang, A. K. Mitra, Y. Zhang, M. Curtis, E. M. Schryver, S. Bettis, A. Jadhav, M. B. Boxer, Z. Li, M. Ferrer and E. Lengyel, *Nat. Commun.*, 2015, **6**, 6220.
31 X. He, P. Liu, H. Zhang, Q. Liao, J. Yao and H. Fu, *Adv. Mater.*, 2017, **29**, 1604510.
32 U. Bog, T. Laue, T. Grossmann, T. Beck, T. Wienhold, B. Richter, M. Hirtz, H. Fuchs, H. Kalt and T. Mappes, *Lab Chip*, 2013, **13**, 2701–2707.
33 H. H. Fang, R. Ding, S. Y. Lu, Y. D. Yang, Q. D. Chen and J. Feng, *Laser Photonics Rev.*, 2013, **7**, 281–288.
34 W. Wang, C. Zhou, T. Zhang, J. Chen, S. Liu and X. Fan, *Lab Chip*, 2015, **15**, 3862–3869.
35 Q. Chen, Y. C. Chen, Z. Zhang, B. Wu, R. Coleman and X. Fan, *Lab Chip*, 2017, **17**, 2814–2820.
36 C. Gong, Y. Gong, Q. Chen, Y. J. Rao, G. D. Peng and X. Fan, *Lab Chip*, 2017, **17**, 3431–3436.
37 M. Huo, L. Wang, Y. Chen and J. Shi, *Nat. Commun.*, 2017, **8**, 357.

38 H. Tan, S. Guo, N. D. Dinh, R. Luo, L. Jin and C. H. Chen, *Nat. Commun.*, 2017, **8**, 663.
39 A. Lin, Q. Hu, C. Li, Z. Xing, G. Ma, C. Wang, J. Li, Y. Ye, J. Yao, K. Liang, S. Wang, P. K. Park, J. R. Marks, Y. Zhou, J. Zhou, M. C. Hung, H. Liang, Z. Hu, H. Shen, D. H. Hawke, L. Han, Y. Zhou, C. Lin and L. Yang, *Nat. Cell Biol.*, 2017, **19**, 238–251.
40 E. S. Bos, A. A. Doelen, N. Rooy and A. H. W. M. Schuurs, *J. Immunoassay*, 1981, **2**, 187–204.
41 D. F. Swinehart, *J. Chem. Educ.*, 1962, **39**, 333.
42 A. B. Aissa, A. Herrera-Chacon, R. R. Pupin, M. D. P. T. Sotomayor and M. I. Pividori, *Biosens. Bioelectron.*, 2017, **88**, 101–108.
43 S. Q. Jin, S. M. Guo, P. Zuo and B. C. Ye, *Biosens. Bioelectron.*, 2015, **63**, 379–383.
44 M. A. Soto, J. A. Ramirez and L. Thévenaz, *Nat. Commun.*, 2016, **7**, 10870.
45 W. J. Tomlinson and C. Lin, *Electron. Lett.*, 1978, **14**, 345–347.
46 Y. J. Rao, *Meas. Sci. Technol.*, 1997, **8**, 355–375.
47 W. C. W. Chan, D. J. Maxwell, X. Gao, R. E. Bailey, M. Han and S. Nie, *Curr. Opin. Biotechnol.*, 2002, **13**, 40–46.
48 R. Gvishi, R. Reisfeld and Z. Burshtein, *Chem. Phys. Lett.*, 1993, **213**, 338–344.
49 http://www.exciton.com/.